Extending Winding Function Theory to Incorporate Secondary Effects in the Design of Induction Machines and Drives

Ge, Baoyun; Liu, Wenbo; Dong, Jianning; Liua, Mingda

DOI
10.1109/JESTPE.2021.3054848

Publication date
2022

Document Version
Accepted author manuscript

Published in
IEEE Journal of Emerging and Selected Topics in Power Electronics

Extending Winding Function Theory to Incorporate Secondary Effects in the Design of Induction Machines and Drives

Baoyun Ge, Wenbo Liu, Jianning Dong, Mingda Liu, *Members, IEEE*

***Abstract*—High performance electric drive applications necessitate a high fidelity model to predict the terminal characteristics of machines in the design stage to fulfill a system level evaluation together with the converters. This paper interprets winding function theory from the field perspective and incorporates secondary effects like slotting and iron nonlinearity into it to accurately predict the main flux linkage in induction machines. The method is centered on resolving the magnetic scalar potential on the two sides of the air gap and computes the flux linkage via winding function. Its performance is benchmarked against 2D finite element analysis and the state of the art magnetic equivalent circuit (MEC) method. Flux linkage and torque results indicate that the relative error is within 3.1% even in highly saturated region when comparing to finite element analysis, while MEC using the same circuit network may present 20% error.**

***Index Terms*—Flux Linkage, Magnetic Circuit Network, Slot Effect, Saturation Effect, Winding Function Theory**

NOMENCLATURE

B_r^{is}, B_r^{or}	Radial component of the magnetic flux density at the stator ID and rotor OD $[\mathrm{T}]$.
C	Number of parallel circuits $[\cdot]$.
$H_\theta^{is}, H_\theta^{or}$	Tangential component of the magnetic field strength at the stator ID and rotor OD $[\mathrm{A/m}]$.
I_i	Current in coil i $[\mathrm{A}]$.
L_{ij}	Mutual inductance between coil i and coil j $[\mathrm{H}]$.
$N^i(\theta)$	Winding function of the coil i $[\cdot]$.
N_{hP}^i	Amplitude of the h-th harmonic of the winding function of the coil i $[\cdot]$.
P	Pole pairs $[\cdot]$.
Q_s, Q_r	Number of stator and rotor teeth $[\cdot]$.
T_e	Electromagnetic torque $[\mathrm{N\text{-}m}]$.
V	Magnetic scalar potential of the teeth $[\mathrm{A}]$.
f, g	Geometric functions $[\cdot]$.
g	Air gap length $[\mathrm{m}]$.
g_{eff}	Effective air gap length $[\mathrm{m}]$.
h	Harmonic order $[\cdot]$.
k_{cs}, k_{cr}	Carter's coefficient at the stator and rotor side $[\cdot]$.
l_e	Effective axial length $[\mathrm{m}]$.
r_{is}, r_{or}	Radius of the stator ID and rotor OD $[\mathrm{m}]$.
α_t, β_t	Center angles (mechanical) of the immediate previous and next slots of the corresponding tooth $[\mathrm{rad}]$.
$\theta, \theta_e, \theta_r$	Mechanical, electrical, and rotor angles $[\mathrm{rad}]$.
λ_{ij}	Mutual flux linkage between coil i and coil j $[\mathrm{Wb}]$.
μ_0	Vacuum permeability $[\mathrm{H/m}]$.
φ	Magnetic scalar potential in the air gap $[\mathrm{A}]$.

Baoyun Ge is with C-Motive Technologies, Inc, Madison, WI, 53704 USA e-mail: baoyun.ge@alumni.com.

Wenbo Liu is with the Ford Motor Company, Deerborn, MI e-mail: wliu89@ford.com.

Jianning Dong is with the Department of Electrical and Computer Engineering, Delft University of Technology, Delft, Neitherland e-mail: J.Dong-4@tudelft.nl.

Mingda Liu is with Carpenter Technology Corp., Philadelphia, PA e-mail: mliu239@wisc.edu.

I. INTRODUCTION

MODERN applications demanding high performance electric drives require an effective prediction of the terminal characteristics of machines in the design stage to fulfill a system level evaluation together with the converters. Secondary effects, like slotting, finite permeability of the iron core, and iron saturation, shall not be ignored. Finite element analysis (FEA) software is usually the ultimate tool for analyzing these effects. Its time consuming nature has driven many researchers to look for alternative methods. These may be categorized into three:

- the first one divides the solving domain into a minimum number of analytically solvable subdomains and numerically resolves the boundary conditions between the subdomains [1]. However, the magnetic nonlinearity and saturation are not yet considered;
- the second one builds magnetic circuit networks upon meshes in the slot and iron regions and deploys analytical solution in the air gap to connect the respective network on the stator and rotor [2], [3]. This is close to finite difference and/or finite element methods given its discretization nature, although it may benefit from no meshes in the air gap in terms of the computational load;
- the third one builds magnetic circuit network as well including the air gap region, but only to the extend capturing the flux path from a high level [4], [5]. It was then integrated in [6] to model the terminal behavior of induction motors under different conditions. Since we will benchmark the proposed method against this method, we will designate it as MEC (magnetic equivalent circuit) following literature's convention. Our benchmark shows that this method is not able to achieve similar accuracy as the proposed one even after incorporating winding function (WF) in the flux computation and Maxwell shear stress tensor in the torque calculation.

This paper is aiming to introduce a new approach different from those. As will be seen later, *in terms of handling the iron core and air gap* our approach here is a hybrid of the latter two methods, i.e. utilizing the analytical solution in the air gap as well as abstracting the iron region as magnetic reluctance. The corresponding gains are preserving largely the spatial harmonics due to slots and reducing greatly the modeling and computational effort, which results in a good balance between accuracy and running cost. *From a broader view*, our approach is closer to winding function theory (WFT) since it is centered on resolving the potential distribution over the stator and rotor surfaces and the calculation of flux linkage relies on WF. MEC, on the other hand, built in [4]–[6] was centered on resolving flux and the winding flux linkage is a direct sum of the flux in each path corresponding to that winding. Therefore, the proposed method is regarded as an extension of WFT in view of the core ideas of solving the field distribution and post-processing.

Simply with the information of the winding layout and gap distance, WFT provides a shortcut to approximate self and mutual inductances [7]–[9]. The magnetomotive force (MMF) is merely the multiplication of WF and the corresponding excitation current. Interestingly though, WFT appeared much later than the MMF concept and it was bred by Novotny and first reported in 1965 [7]. Nevertheless, WFT is quite powerful when aforementioned secondary effects can be dropped. Toliyat employed it in the modeling and harmonic analysis of induction machines [10]. His approach was then extensively applied in machines under winding fault [11], [12] or with eccentric rotors [13]. One may refer to the detailed review of these applications and modification on WFT presented in [14].

In its default definition, WFT is not intuitively ready to account these non-ideal effects. Therefore, in Section II, WFT is revisited and then explained from a different perspective. Along the way, a generalization to accommodate large air gap machines is also made from the new perspective. These secondary effects are then linked with the alternative explanation of WFT using the topology of induction machines as an example in Section III followed by Section IV presenting computational subtleties. It is then benchmarked against 2D FEA and MEC from [4]–[6] in terms of flux linkage, torque evaluation, air gap flux density, and computational cost in Section V.

It is worth to mention that the proposed approach tackles these secondary effects as classic techniques in the machine design practice:

- the slot effect is usually taken care of by applying Carter's coefficient on the air gap length [15];
- the finite permeability of the iron core diminishes the total disposable MMF from the excitation. Normally, magnetic circuits shall be drawn and solved in a preliminary design prior to finite element analysis (FEA) [16], [17];
- the iron saturation or generally the magnetic nonlinearity can be included in the magnetic circuit analysis with iterative algorithms. An extremely simple case would be determining the working point of a C-core inductor with a graph method [16].

Therefore, the proposed approach may be well integrated into a graduate-level machine design course in view of the increasing demand in evaluating electric drive performance when the time that would be consumed by FEA is not acceptable.

Lastly, we would like to point out that the approach here overlaps with MEC *on* setting up the magnetic circuitry of the iron region [4]–[6]. Only the core ideas conceived by us are presented next for conciseness, and the full picture is captured in the narrative and especially two proposed algorithms.

II. WFT from A Different Perspective

A. Revisit WFT

Generally, WF for machines with uniform air gap is defined as

$$N(\theta) = n(\theta) - \langle n(\theta) \rangle. \tag{1}$$

The function $n(\theta)$ is cumulative along the angular direction in the air gap such that it accumulates the number of turns as well as registers the direction of every winding it encounters. The angled brackets denote the averaging operation over the interval where $n(\theta)$ is defined, therefore the mean value of $N(\theta)$ is forced to zero. This operation, in line with the principal of minimum energy (PME), ensures the correctness of the resultant inductances and also allows one to start $n(\theta)$ with an arbitrary number at an arbitrary position.

With the above definition, WFT states that the mutual inductance between two sets of windings i and j in an *induction machine* can be approximated as

$$L_{ij} = \frac{r l_e}{I_j} \int_0^{2\pi} N^i(\theta_e) B_r^j(\theta_e)\, d\theta_e \cdot \frac{1}{C^2} \tag{2a}$$

$$= \frac{\mu_0 r l_e}{g} \int_0^{2\pi} N^i(\theta_e) N^j(\theta_e)\, d\theta_e \cdot \frac{1}{C^2}, \tag{2b}$$

where g is the gap length, r is the mean radius of the gap, l_e is the effective axial length, C is the number of parallel circuits, θ_e is the electrical angle in radians, $N^i(\theta_e)$ and $N^j(\theta_e)$ are the corresponding winding functions, and $B_r^j(\theta_e)$ is the radial component of the flux density distribution in the air gap caused by the current I_j in winding j [7]–[9]. When i and j represent the same winding, it becomes the formula for the self inductance of that winding if we ignore all the leakage flux. The significance of eqs. (2a) and (2b) is that the definition of WF allows the integration interval to be $[0, 2\pi]$. Equation (2b) is commonly used since $B_r^j(\theta_e)$ is obtained with the knowledge of $N^j(\theta_e)$, although one has to be aware that $N^i(\theta_e)$ counts for the physical layout of the winding i while $N^j(\theta_e)$ is representing the pattern of the field generated by the current in winding j. In the special situation that WF is derived, $N^i(\theta_e)$ and $N^j(\theta_e)$ are reciprocal, inline with the reciprocity of mutual inductance.

For conciseness, we will limit our analysis to the two windings i and j only. However, our method is capable of handling multiple windings, which will be verified in Section V.

B. Incorporate Air Gap Transfer Relation

Obviously, the information of the slots, absolute excitation current, and magnetic property of the iron core is not encoded

in $N^j(\theta_e)$. To count the secondary effects, we need to look at Equation (2a) instead. Actually, one more step back is indispensable. The saturation effect makes the system nonlinear and we are forced to drop the definition of inductance and use the more generic term — flux linkage [7]:

$$\lambda_i = rl_e \int_0^{2\pi} N^i(\theta_e) B_r^j(\theta_e)\, d\theta_e \cdot \frac{1}{C^2}. \tag{3}$$

The work is then focused on finding $B_r^j(\theta_e)$ to determine the terminal characteristic $\lambda_i(I_j)$. The method proposed in [2], [3] and reviewed in the introduction can serve the purpose and yield high accuracy with decent mesh density, however its computational complexity counteracts the conciseness of WFT. MEC from [4]–[6] computes the winding flux linkage by summing the flux in each path corresponding to that winding, which results in large error even in the linear region of the back iron as shown in Section V. After incorporating WF, its accuracy is substantially improved in the linear region. However, it still does not correlate well with FEA when the iron is saturated. Our method relies on the air gap transfer relation documented in [18] to obtain an accurate representation of the flux density $B_r(\theta_e)$ in the air gap:

$$\begin{bmatrix} \widetilde{B}_r^{is} \\ \widetilde{B}_r^{or} \end{bmatrix} = j\mu_0 \begin{bmatrix} f(r_{or}, r_{is}, hP) & g(r_{is}, r_{or}, hP) \\ g(r_{or}, r_{is}, hP) & f(r_{is}, r_{or}, hP) \end{bmatrix} \begin{bmatrix} \widetilde{H}_\theta^{is} \\ \widetilde{H}_\theta^{or} \end{bmatrix}, \tag{4}$$

where P is the number of pole pairs, tildes indicate phasors of the h-th harmonic, superscripts is and or denote the location of the field, i.e. stator ID and rotor OD, and the geometric functions f and g are defined as

$$f(x, y, m) = \frac{(x/y)^m + (y/x)^m}{(x/y)^m - (y/x)^m}, \tag{5}$$

$$g(x, y, m) = \frac{2y/x}{(x/y)^m - (y/x)^m}, \tag{6}$$

and they may be replaced the hyperbolic functions $\sinh(Pg/r)$ and $\cosh(Pg/r)$ when $Pg \ll r$. One may refer to [18] for their geometric meanings. At first sight, it seems that the flux density B is just written in terms of the field strength H. The advantageous consequence is actually the shifting from the radial direction to the circumferential direction as signified by the subscripts. Recall that the magnetic field in the air gap region is current free and may be described by the scalar potential

$$H_\theta = -\frac{1}{r}\frac{\partial \varphi}{\partial \theta} \quad or \quad \widetilde{\varphi} = jr\widetilde{H}_\theta / hP, \tag{7}$$

where r is the radius of the position under consideration. Therefore, with the knowledge of the distribution of $\varphi(\theta_e)$ in the air gap, one can obtain the flux linkage for any windings (leakage flux is set aside for now and will be discussed in Section V). If one refers to Figure 1, it is actually inline with the well accepted eq. (2b) since the potential $\varphi(\theta_e)$ is exactly $N^j(\theta_e)$ multiplied by the excitation current I_j. When the secondary effects are counted, the actual distribution of $\varphi(\theta_e)$ differs from $N^j(\theta_e)I_j$. Sections III and IV will detail the steps of computing the "lost" ampere-turns from $N^j(\theta_e)I_j$.

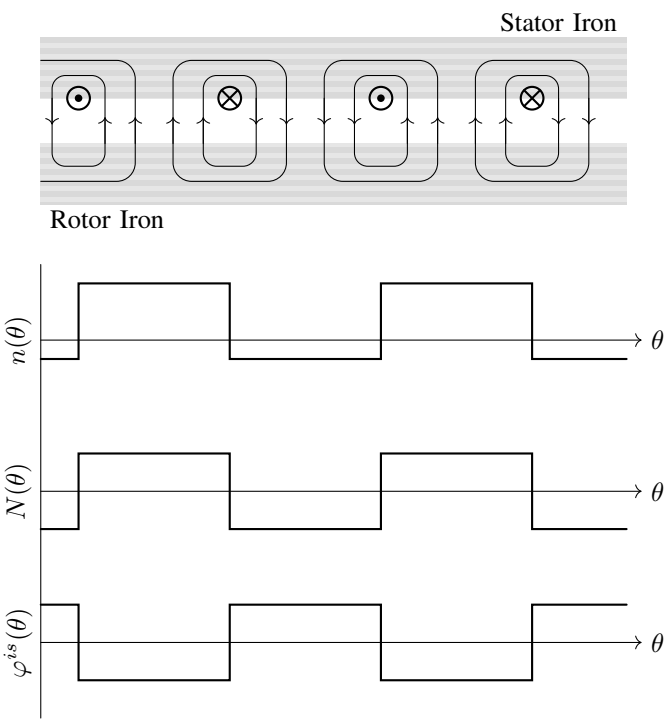

Fig. 1: Re-illustrating the concept of WF. The iron permeability is assumed to be infinite. The function $n(\theta)$ is defined such that it adds turns when the winding points out of the paper.

Before ending this section, we would like to remark that eq. (2b) (of classic WFT) may cause more error when the gap length is not trivial comparing to the average radius r. Instead, eqs. (4) and (7) should be used together with eq. (2a). For example, when winding i is on the stator side, the self inductance may be computed as

$$L_{ii} = \frac{\pi \mu_0 l_e P}{C^2} \sum_{h=1,3}^{\infty} hf(r_{is}, r_{or}, hP)(N_{hP}^i)^2, \tag{8}$$

where N_{hP}^i is the amplitude of the h-th harmonic of WF of the winding i.

III. Linking WFT with the Secondary Effects

For the purpose of illustrating the process and verifying the method, the induction machine model shown in Figure 2 is assumed for the rest of the paper. The authors are working on adapting the method to other common types of machines.

A. Slot Effect

As affirmed in Section II-B, the goal is to look for the distribution of $\varphi(\theta_e)$ at the two sides of the air gap, i.e. $\varphi^{is}(\theta_e)$ and $\varphi^{or}(\theta_e)$. Due to the high permeability contrast between the iron and the air (even under non-excessive saturation), the magnetic potential on the teeth surface may be regarded as constants. Therefore, what is left is to model the slot. We are proposing two ways, i.e. using simply Carter's coefficient or conformal mapping (CM) from the ground up, and using a configuration of misaligned facing slots shown in Figures 3 and 4 to describe them.

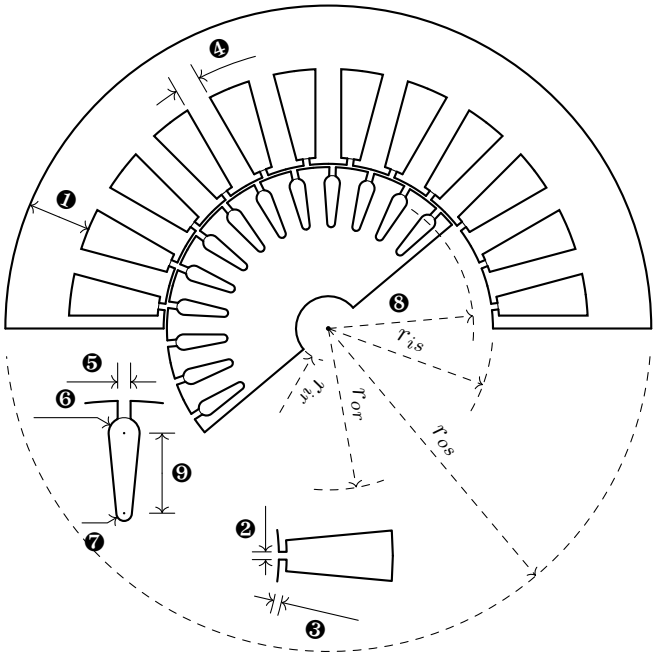

Fig. 2: A 4-pole induction machine with 24 stator slots and 26 rotor slots. The depicted rotor position is $2\pi/9\,\mathrm{mech.\ rad}$. The labeled dimensions are explained in Table I.

1) Using Carter's Coefficient: The simplest way of representing the magnetic potential over the slots may be a linear interpolation between the teeth potential, which is shown in Figure 3. However, this is quite different from the true distribution (see Figure 4) and will not result in the correct flux representing going into/out of the teeth (refer to Section III-B) after applying eq. (4). Carter's coefficient was derived for correcting this error [15] and is usually used in another way, i.e. obtaining the effective air gap. Designating k_{cs} and k_{cr} as the stator and rotor Carter's coefficients, the radius r_{is} and r_{or} in eq. (4) may be replaced respectively by effective ones

$$r_{is,eff} = r_{is} + (k_{cs}k_{cr} - 1)g/2 \tag{9}$$

and

$$r_{or,eff} = r_{or} - (k_{cs}k_{cr} - 1)g/2. \tag{10}$$

This route is relatively easy to implement and slightly more time efficient than the next one. However, the harmonic information of $\widetilde{B}_r$ and $\widetilde{H}_\theta$ is not genuinely represented because of the linearization step.

2) Using Conformal Mapping: If we trace back to how Carter's coefficient was derived in the first place, we would find that the magnetic potential distribution over the slots can be solved using CM for the single slot configuration [15]. For two slots facing each other (and most likely misaligned), there is no reported explicit mapping equation. However, this may be tackled by using the numerical Schwarz-Christoffel toolbox [19]. The application procedures were documented in [20] and will be omitted here.

This may not seem to be time efficient since the computational cost of CM is high and it has to be done repetitively at different rotor positions. A workaround may be realized if

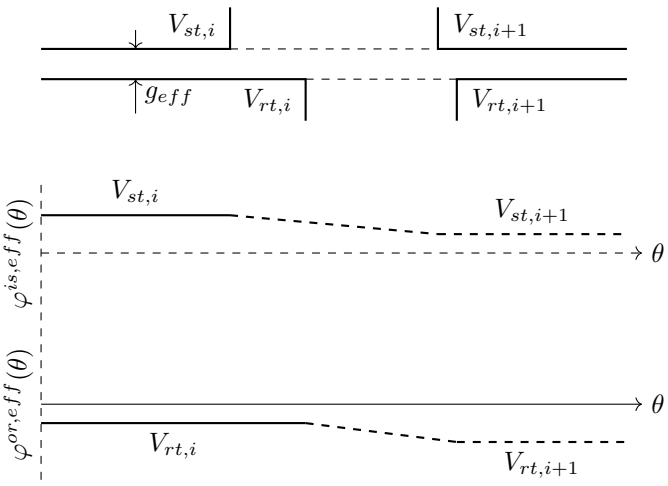

Fig. 3: Modeling the slot effect by linearly interpolating the magnetic potential. Carter's coefficient is used to obtain the effective gap length $g_{eff} = k_{cs}k_{cr}g$. To eliminate confusion, the symbol V instead of φ is used to denote potential on the teeth. Subscripts st and rt indicate stator tooth and rotor tooth.

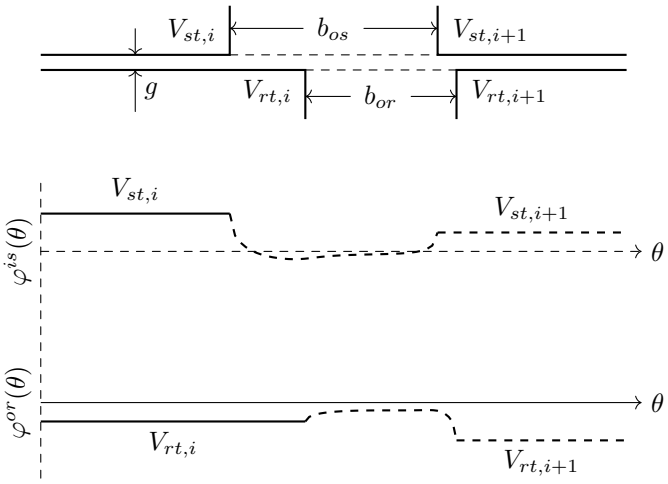

Fig. 4: Modeling the slot effect by calculating the potential distribution using weighting coefficients obtained from CM.

one observes that the magnetic potential distribution is a linear combination of the four teeth potential, i.e.

$$\varphi^{is}(\theta) = k_{st,i}(\theta)V_{st,i} + k_{st,i+1}(\theta)V_{st,i+1} + k_{rt,i}(\theta)V_{rt,i} + k_{rt,i+1}(\theta)V_{rt,i+1}. \tag{11}$$

These weighting coefficients $k_{st,i}(\theta)$, $k_{st,i+1}(\theta)$, $k_{rt,i}(\theta)$, and $k_{rt,i+1}(\theta)$ are functions of the air gap length g, slot openings b_{os} and b_{or}, and the misalignment Δb_o. They can be obtained by setting $V_{st,i}$, $V_{st,i+1}$, $V_{rt,i}$, and $V_{rt,i+1}$ respectively to 1 A-t and the rest to zero. The same applies for $\varphi^{or}(\theta)$. To efficiently obtain $\varphi^{is}(\theta)$ and $\varphi^{or}(\theta)$ during runtime, one may use the aforementioned toolbox to sweep the space formed by b_{os}/g, b_{or}/g, and $\Delta b_o/g$, store the coefficients in a look up table, and interpolate them during runtime. The sweeping only needs to be done once and can be carried to other induction machine designs.

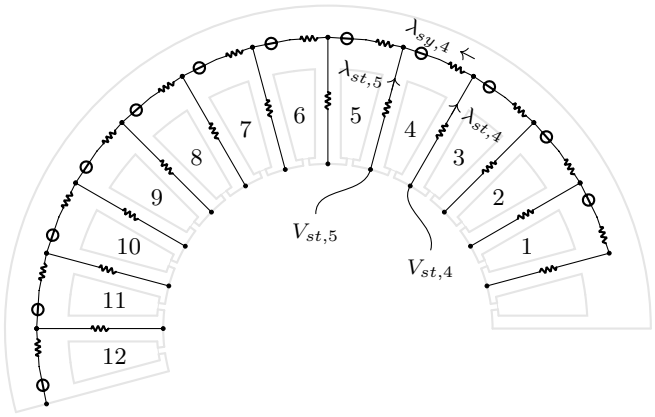

Fig. 5: Stator side magnetic circuit network of the induction machine. The circular components are the MMF sources $\mathcal{F}_{s,i}$ for each slot. The fourth slot is singled out to illustrate Algorithm 1. One more slot from the second pole pair is added to show the boundary element. Rotor side is handled in the same way, more or less a mirror image.

B. MMF Drop on Iron

We will temporarily assume $\varphi^{is}(\theta_e)$ and $\varphi^{or}(\theta_e)$ are available after modeling the slot effect and Section IV will present an algorithm for these to iterate and converge. As mentioned before, we may use eqs. (4) and (7) to restore the radial component of the flux density in the air gap. The flux into/out of any tooth is then readily computed as

$$\lambda_t = r l_e \int_{\alpha_t}^{\beta_t} B_r(\theta)\, d\theta, \tag{12}$$

where α_t and β_t are the center angles of the immediate previous and next slots of the tooth. (If $B_r(\theta)$ preserves the direction definition in eq. (4), then the flux computed from eq. (12) is out of the tooth for the rotor side.)

All the flux into the teeth are fed into the stator (shown in Figure 5) and rotor magnetic circuit networks. The networks are set up similarly to [4]–[6].

If the magnetic material is linear or it is working in the linear region, these reluctances in the networks are readily known and one may set up a set of linear equations to resolve the MMF drop as in [4]–[6].

C. Nonlinearity and Saturation Effects

If the material is nonlinear, a numerical method should be applied to obtain the MMF drop since the reluctances (the permeability part) are inexplicit functions of the flux density and thus flux flow at the intersections (from teeth to yokes) cannot be determined explicitly. Referring to the stator side network in Figure 5, Algorithm 1 is proposed to determine the MMF drop $\Delta V_{ss,i}$ on iron around the i-th stator slot (denoted as ss). It takes advantage of the simple structure of the network (which in fact is sufficient) and relies on the fact that the potential drop on the yoke loop is zero.

Obviously, if the teeth surface potential $V_{st,i}$ and $V_{rt,i}$ were *not* genuinely represented, the potential drop calculated from

Algorithm 1: Find MMF Drop on Iron

input : Flux injected into each stator tooth $\lambda_{st,i}$, MMF of each slot $\mathcal{F}_{s,i}$, iron magnetic property $B = B(H)$, width w_{st}, w_{sy} and depth d_{st}, d_{sy} of the lumped reluctances, and machine axial length l_e.

output: Potential drop around each slot $\Delta V_{ss,i}$.

interpolate the H field in the teeth from $\lambda_{st,i}/w_{st}l_e$ using $B = B(H)$;

compute the potential drop on each tooth via multiplying the H field by d_{st};

`/* now compute the potential drop on each yoke */`

pick a yoke path (say the 4th one) and initialize its flux $\lambda_{sy,4}$;

loop until the terminal condition is met

  compute the flux $\lambda_{sy,i}$ in other yokes according to Kirchhoff's current law;

  interpolate the H field in the yokes from $\lambda_{sy,i}/w_{sy}l_e$ using $B = B(H)$;

  compute the potential drop on each yoke via multiplying the H field by d_{sy} and sum them up;

  if *the sum is small enough* **then**

    break;

  else

    use the secant method to determine the next value for $\lambda_{sy,4}$;

  end

end

compute the potential drop around each slot including one yoke, two teeth elements, and the corresponding MMF source $\mathcal{F}_i$;

return.

Algorithm 1 would violate the following equations arising from Ampere's law for at least one slot:

$$\Delta V_{ss,i} = V_{st,i} - V_{st,i+1},\ 1 < i < Q_s \tag{13}$$

or

$$\Delta V_{rs,i} = V_{rt,i} - V_{rt,i+1},\ 1 < i < Q_r \tag{14}$$

where Q_s and Q_r are the number of stator and rotor slots respectively. The next section will present an iterative method for these teeth potential to converge.

IV. Iteration Method

According to the conditions in eqs. (13) and (14), a multivariable function F is constructed as

$$F = [F_{s,1}; F_{s,2}; \ldots; F_{s,Q_s}; F_{r,1}; F_{r,2}; \ldots; F_{r,Q_r}], \tag{15}$$

where

$$F_{s,i} = \begin{cases} \Delta V_{ss,i} - (V_{st,i} - V_{st,i+1}) & i \neq Qs \\ \langle \varphi^{is}(\theta) \rangle & i = Qs \end{cases}, \tag{16}$$

$$F_{r,i} = \begin{cases} \Delta V_{rs,i} - (V_{rt,i} - V_{rt,i+1}) & i \neq Qr \\ \langle \varphi^{or}(\theta) \rangle & i = Qr \end{cases}. \tag{17}$$

Algorithm 2: Find Stator and Rotor Teeth Potential

input : Machine design parameters, iron magnetic property $B = B(H)$, excitation current.
output: $V_{st,i}$ $(1 < i < Q_s)$ and $V_{rt,i}$ $(1 < i < Q_r)$.

initialize $V_{st,i}$ and $V_{rt,i}$ according to the excitation current assuming the back iron consumes no MMF;
loop until the terminal condition is met
  get the potential distribution at the stator ID and rotor OD according to Section III-A;
  compute function F and its norm $||F||_2$ using Algorithm 1 and eqs. (15) to (17);
  if $||F||_2$ *is small enough* **then**
    return;
  else
    update $V_{st,i}$ and $V_{rt,i}$ using the Jacobian matrix of F, which may be obtained through Broyden's method [21];
  end
end

Again, the angled brackets denotes the averaging operation over $[0, 2\pi]$ as in eq. (1). The reason for the special treatment when $i = Q_s$ and $i = Q_r$ is that the total current in either the stator or the rotor side are summed zero. Satisfying Ampere's law in the first $(Q_s - 1)$ and $(Q_r - 1)$ slots will automatically ensure the last ones. At the same time, PME requires $\langle \varphi^{is}(\theta) \rangle$ and $\langle \varphi^{or}(\theta) \rangle$ to be zero.

The goal is to find the right stator and rotor teeth potential so that $||F||_2 = 0$, where the subscript denotes the Euclidean norm. Algorithm 2 is proposed to accomplish this and it also serves as an overview of the whole solving process. Intuitively, the updating step may be categorized into the following two cases:

- teeth potential is too large, which results in larger flux into/out the teeth and thus higher MMF drop in the iron;
- teeth potential is too small, which results in smaller flux into/out the teeth and thus lower MMF drop in the iron.

Both cases end with correcting the excessive estimation of the teeth potential. One may also use the C-core inductor mentioned in the introduction as an example to understand the process except the dimension herein is $(Q_s + Q_r)$ instead of one.

V. Comparison Study with FEA and MEC

The reader may have noticed that the proposed approach concerns only the main flux distribution. Indeed, the leakage flux are well covered in the textbook [16], [17] and may be incorporated in parallel (refer to the first case study in Section V-A). It is thus more appropriate to benchmark the approach against FEA, which can easily segregate the main flux from the leakage one and evaluate the gap field distribution. Experiments with prototypes are beneficial in evaluating the overall system performance and will be deferred to future publications. Nevertheless, MEC from [4]–[6] is included in the case studies below and its stator and rotor magnetic circuits are set up with exactly the same parameters as the proposed approach. Four aspects will be verified against, i.e. main flux linkage, torque evaluation, air gap flux density, and computational time. The first two are the state variables in evaluating system dynamics and therefore their accuracy is critical.

TABLE I: Parameters of the Simulated Induction Machine. Dimension labels correspond to Figure 2. The slot fill factor is defined as the ratio of the copper area to the slot area.

Name	Value	Name	Value
Pole pairs	2	Parallel circuits	1
Stator slot #	24	Rotor bar #	26
Coil pitch	6	Turns per coil	60
Slot fill factor	0.71	Stator core depth ❶	10.47 mm
Stator OD, $2r_{os}$	106.8 mm	Stator slot width ❷	1.068 mm
Stator ID, $2r_{is}$	54.46 mm	Stator teeth width ❸	4.271 mm
Rotor ID, $2r_{ir}$	10.68 mm	Stator tang depth ❹	1.068 mm
Rotor OD, $2r_{or}$	53.39 mm	Rotor slot width ❺	1.07 mm
Gap length	0.535 mm	Outer bar radius ❻	1.28 mm
Stack length	106.8 mm	Inner bar radius ❼	0.64 mm
Bar outer center depth ❽	2.67 mm	Bar edge center distance ❾	6.62 mm

An induction machine generated from JMAG-Express Online [22] with the constraints $7.46\,\mathrm{kW}$ and $1800\,\mathrm{rpm}$ is used through out the case studies. Its geometric parameters are given in Table I. The very common lamination material M19 with a stacking factor of 0.93 is assumed for the back iron.

A. Main Flux Linkage

In this first study, only coil A is excited and its corresponding flux linkage is extracted as a function of the excitation level, which is shown in Figure 6. The first three are calculated via: 1) energy method [7]; 2) adding the leakage inductance [17] multiplied by the excitation current to the proposed one; 3) integrating the simulated flux density multiplied by WF as in the proposed approach. The two MEC lines are based on [4]–[6] with discrete lumped air gap permeances. For ①, the flux linkage is a sum over the corresponding teeth and for ②, it is calculated using WF like the proposed method here after obtaining the tooth potential from the resolved network. The last one takes the stacking factor into account in 3D FEA. The proposed one uses CM to model the slot. The route using Carter's coefficient results in indistinguishable difference and is thus omitted.

As mentioned above, the proposed approach deals with the main flux only. Particularly, the slot leakage is not included in the circuit network shown in Figure 5. (The MEC network in [4]–[6] covers the leakage partially, i.e. the tang part.) It is however easier and computationally more effective to simply add this term after computing the main flux, which is shown in Figure 6 and proved to have a relative error less than 3.1%. When slot leakage is excluded, FEA results in slightly higher value than the proposed one with high current. The reason is that the proposed approach models the slot effect with the assumption that the teeth is infinitely permeable, which is no longer true when the iron gets saturated. This can also be observed from Figures 8 and 9 shown in Section V-C. The MEC method is effective in predicting the general trend, but

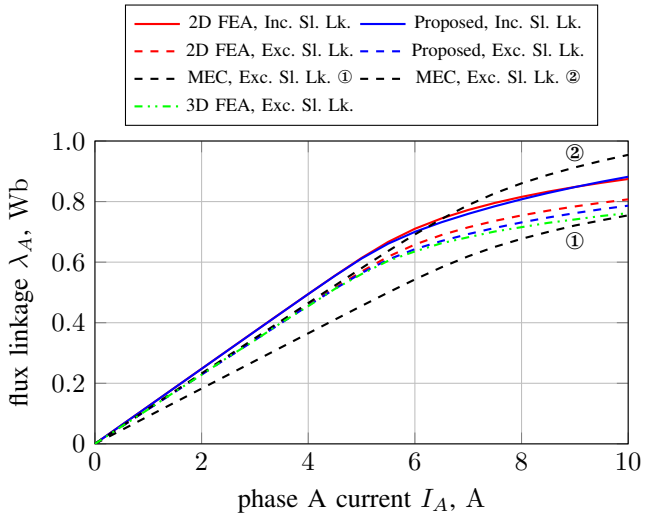

Fig. 6: Phase A flux linkage as a function of its excitation current (rotor position is 0 mech. rad).

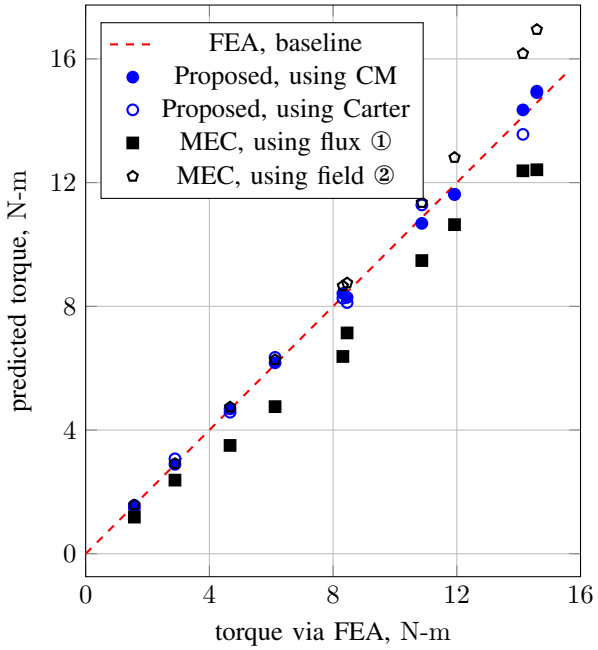

Fig. 7: Predicted electromagnetic torque against FEA results. (The extracted current and rotor position data are provided in Table III in the appendix.)

the accuracy is not acceptable in high performance applications. Especially in the linear region, the relative error is as large as 20% (① vs FEA). After using WF to calculate the flux linkage (i.e. ②), the linear region correlates well with the other two, however it starts to deviate once entering the saturation region. Part of the reason is due to the lack of accounting the fringing field. A hybrid approach combining MEC and FEA is proposed in [23] to model the fringing effect. However, the fringing effect was modeled through fitting the result from FEA, which could be a time consuming process.

The stacking factor effect on the flux linkage in Figure 6 is expected as the insulation material may be regarded as fully saturated steel (like air magnetically) and the effective saturation level is higher than without the insulation layer. Nonetheless, the relative error of the proposed method to the 3D FEA is still less than 3%. Given the complexity of modeling this lamination layer, the stacking factor effect will be incorporated in the future work of the proposed method.

B. Torque Evaluation

In the second study, all three phases and the rotor bars are excited. A simple plot like Figure 6 is not attainable because the flux linkage of each winding is a multivariable functions of all the currents in the stator windings and rotor bars. Instead, the electromagnetic torque, as an important state variable in system dynamics, is evaluated. Ten load torque were picked evenly from zero to 15 N-m and applied in FEA for a line-start simulation. Then the winding and bar currents and rotor positions were extracted at the time $t = 1$ s (all load conditions approached steady state with some torque ripple at this time) and used as input to the proposed and MEC algorithms. The results are documented in Figure 7. The proposed approach obtains the torque via integrating Maxwell shear stress tensor (see eq. (4)) over the rotor surface. The last two, again, are based on [4]–[6] with discrete lumped air gap permeances. For ①, the torque is computed using the formular $T_e = (2P/3)\Im[(i_a + \bar{a}i_b + \bar{a}^2 i_c)(\lambda_a + \bar{a}\lambda_b + \bar{a}^2\lambda_c)^*]$, where $\bar{a} = e^{j2\pi/3}$ [6], [8]. For ②, it is calculated through Maxwell shear stress tensor after obtaining the tooth potential and the H_θ and B_r field from the resolved network. Notice that the electromagnetic torque does not equal to the applied load, which is evenly picked from zero to 15 N-m, due to the unavoidable torque ripple. Similar conclusions can be reached as in the last case study and will be omitted here.

C. Air Gap Flux Density

Two working conditions from Sections V-A and V-B are selected respectively to show the effect of saturation on the predicted air gap flux density. Specifically, the end of the linear region $I_A = 5$ A and the most saturated point $I_A = 10$ A are picked from Figure 6, and one light load condition $T_L = 7.5$ N-m and one heavy load condition $T_L = 15$ N-m are picked from Figure 7. These are plotted in Figures 8 to 11. The harmonic content is counted up to 301 for non-FEA methods. One may immediately tell that the B_r field is indeed, as expected from Figure 6, better predicted in the proposed method under saturation from Figure 9. This is, however, not obvious in Figure 11. Most of the torque are generated on the tooth edges and thus one need to focus on the slot region transition to see why the proposed one is better than MEC in terms of predicting the electromagnetic torque.

In the last three case studies, the well agreement between FEA and the proposed method may be attributed to: 1) the use of air gap transfer relation rather than lumped permeances in MEC; 2) the high fidelity modeling of the slot effect using CM rather than zero permeances between slots and teeth as in MEC.

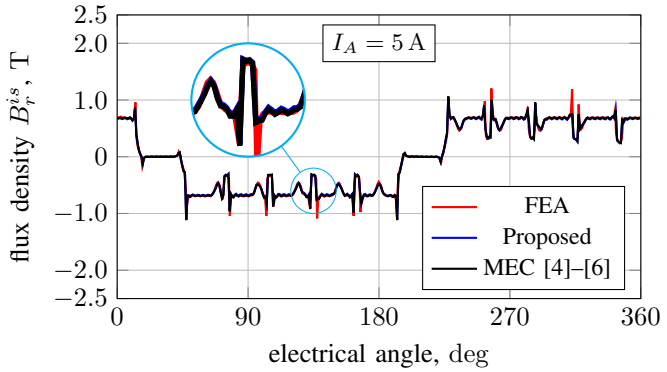

Fig. 8: The radial component of flux density at the radius $r = r_{is}$ as a function of electrical angle. This corresponds to 5 A in Figure 6.

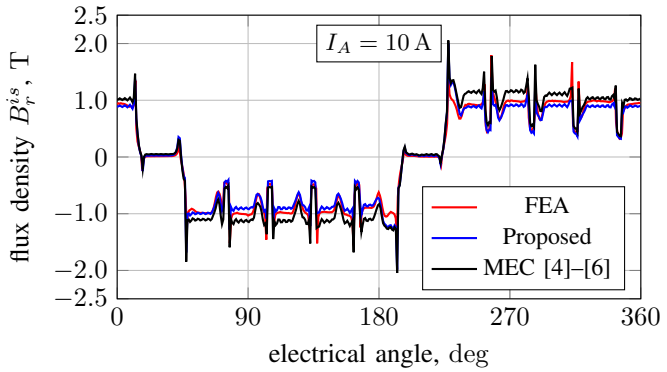

Fig. 9: The radial component of flux density at the radius $r = r_{is}$ as a function of electrical angle. This corresponds to 10 A in Figure 6.

TABLE II: Summary of Average Computational Time.

for	FEA	MEC	Proposed	
			w/ Carter's Coef.	w/ CM
Case Study A	23 s	0.33 s	0.40 s	0.53 s
Case Study B	63 s	0.45 s	0.48 s	0.60 s

D. Summary of Computational Time

Table II documents the average computational time for the case studies presented in Sections V-A and V-B. The proposed approach using CM is slightly slower than MEC. Potentially, this may be improved via a combination of the two proposed routes, i.e. using Carter's coefficient to model the slot effect at the beginning of the iteration and switching to CM towards the end after $||F||_2$ becomes small enough. It is also worth to mention that the non-FEA ones are conducted in an interpreted language environment. Had the approaches been implemented in a C/Fortran environment, the time cost would be much lower.

VI. Conclusion and Future Work

This paper proposed an effective method to predict the terminal characteristic of induction machines when secondary effects like slotting and iron nonlinearity *cannot* be ignored.

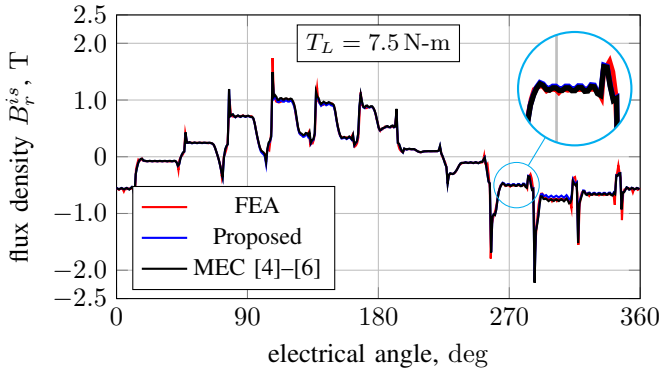

Fig. 10: The radial component of flux density at the radius $r = r_{is}$ as a function of electrical angle. This corresponds to 7.5 N-m load torque in Figure 7.

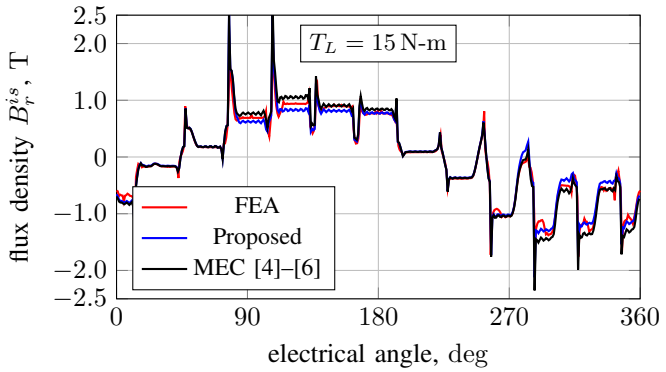

Fig. 11: The radial component of flux density at the radius $r = r_{is}$ as a function of electrical angle. This corresponds to 15 N-m in Figure 7.

It relies on the analytical solution in the air gap region and models the back iron using magnetic circuit networks. The solving process is centered on resolving the magnetic scalar potential at the ID and OD of the stator and rotor respectively and the flux linkage is computed using WF, due to both of which the proposed method is regarded as an extension of WFT. Specifically, this paper contributes the following to the state of the art:

- WFT is explained from the field perspective, which enables the proposed method (Section II).
- a generalization of WFT to cover large air gap effects using the analytical solution in the air gap (Section II);
- two numerical ways of handling the slot effect based on magnetic scalar potential are proposed (Section III-A);
- two effective algorithms are proposed to iterate the magnetic scalar potential distribution on the stator ID and rotor OD (Algorithms 1 and 2);
- the overall approach is benchmarked against 2D FEA and compared to the state of the art method with similar computational cost [4]–[6]. The result shows that the relative error of the predicted flux linkage and electromagnetic torque is within 3.1% even in highly saturated region and the computational cost is slightly higher than MEC (Section V), which makes it suitable for the machine

design optimization;

- the spatial harmonics are largely preserved in the proposed method, which may enable high fidelity modeling of other secondary effects like cogging torque, unbalanced magnetic pull, eddy current iron loss, etc.

The proposed method is directly applicable to non-salient type synchronous machines as well. Going forward, the proposed method will be adapted further in other common types of electrical machines, such as salient-pole synchronous machines and permanent magnet synchronous machines. Furthermore, it is the authors' intention to integrate this method in a graduate-level electric machine design course since the central elements of this method are all well covered in the canon of machine design practice and the demand for high fidelity model is increasing as illustrated in the introduction.

APPENDIX
DATA USED FOR THE CASE STUDY IN SECTION V-B

ACKNOWLEDGMENT

The authors would like to thank Dr. D. W. Novotny for sharing the WFT history, specifically on how it was conceived in the first place.

REFERENCES

[1] Y. Oner, Z. Q. Zhu, L. J. Wu, X. Ge, H. Zhan, and J. T. Chen, "Analytical On-Load Subdomain Field Model of Permanent-Magnet Vernier Machines," *IEEE Transactions on Industrial Electronics*, vol. 63, no. 7, pp. 4105–4117, Jul. 2016.

[2] H. Ghoizad, M. Mirsalim, Ieee, M. Mirzayee, and W. Cheng, "Coupled magnetic equivalent circuits and the analytical solution in the air-gap of squirrel cage induction machines," *International Journal of Applied Electromagnetics and Mechanics*, vol. 21, pp. 1–6, Jan. 2005.

[3] K. J. W. Pluk, J. W. Jansen, and E. A. Lomonova, "Hybrid Analytical Modeling: Fourier Modeling Combined With Mesh-Based Magnetic Equivalent Circuits," *IEEE Transactions on Magnetics*, vol. 51, no. 8, pp. 1–12, Aug. 2015.

[4] V. Ostovic, "A Method for Evaluation of Transient and Steady State Performance in Saturated Squirrel Cage Induction Machines," *IEEE Transactions on Energy Conversion*, vol. EC-1, no. 3, pp. 190–197, Sep. 1986.

[5] ——, "A simplified approach to magnetic equivalent-circuit modeling of induction machines," *IEEE Transactions on Industry Applications*, vol. 24, no. 2, pp. 308–316, Mar. 1988.

[6] S. D. Sudhoff, B. T. Kuhn, K. A. Corzine, and B. T. Branecky, "Magnetic Equivalent Circuit Modeling of Induction Motors," *IEEE Transactions on Energy Conversion*, vol. 22, no. 2, pp. 259–270, Jun. 2007.

[7] N. L. Schmitz and D. W. Novotny, *Introductory Electromechanics*. Ronald Press, 1965.

[8] D. W. Novotny and T. A. Lipo, *Vector Control and Dynamics of AC Drives*, 1st ed. Oxford : New York: Clarendon Press, Sep. 1996.

[9] T. A. Lipo, *Analysis of Synchronous Machines*. Wisconsin Power Electronics Research Center, University of Wisconsin, 2008.

[10] H. A. Toliyat, "Analysis of Concentrated Winding Induction and Reluctance Machines for Adjustable Speed Drive Applications," Ph.D. dissertation, University of Wisconsin-Madison, 1991.

[11] X. Luo, Y. Liao, H. Toliyat, A. El-Antably, and T. Lipo, "Multiple coupled circuit modeling of induction machines," *IEEE Transactions on Industry Applications*, vol. 31, no. 2, pp. 311–318, Mar. 1995.

[12] H. Toliyat and T. Lipo, "Transient analysis of cage induction machines under stator, rotor bar and end ring faults," *IEEE Transactions on Energy Conversion*, vol. 10, no. 2, pp. 241–247, Jun. 1995.

[13] N. Al-Nuaim and H. Toliyat, "A novel method for modeling dynamic air-gap eccentricity in synchronous machines based on modified winding function theory," *IEEE Transactions on Energy Conversion*, vol. 13, no. 2, pp. 156–162, Jun. 1998.

[14] L. Serrano-Iribarnegaray, P. Cruz-Romero, and A. Gomez-Exposito, "Critical Review of the Modified Winding Function Theory," *Progress In Electromagnetics Research*, vol. 133, pp. 515–534, 2013.

[15] F. W. Carter, "The magnetic field of the dynamo-electric machine," *Journal of the Institution of Electrical Engineers*, vol. 64, no. 359, pp. 1115–1138, Nov. 1926.

[16] T. A. Lipo, *Introduction to AC Machine Design*, 2nd ed. Madison, WI: University of Wisconsin-Madison, Aug. 2007.

[17] J. Pyrhonen, T. Jokinen, and V. Hrabovcova, *Design of Rotating Electrical Machines*, 1st ed. Chichester, West Sussex, United Kingdom ; Hoboken, NJ: Wiley, Feb. 2009.

[18] J. R. Melcher, *Continuum Electromechanics*, 1st ed. Cambridge, Mass: The MIT Press, Jun. 1981.

[19] "Schwarz-Christoffel Toolbox," http://www.math.udel.edu/~driscoll/SC/.

[20] T. C. O'Connell and P. T. Krein, "A Schwarz-Christoffel-Based Analytical Method for Electric Machine Field Analysis," *IEEE Transactions on Energy Conversion*, vol. 24, no. 3, pp. 565–577, Sep. 2009.

[21] J. E. Dennis and R. B. Schnabel, *Numerical Methods for Unconstrained Optimization and Nonlinear Equations*, ser. Classics in Applied Mathematics. Society for Industrial and Applied Mathematics, Jan. 1996.

[22] "JMAG-Express Online [Free Software]," https:/www.jmag-international.com/express/.

[23] J. Lannoo, D. Vanoost, J. Peuteman, S. Debruyne, H. D. Gersem, and D. Pissoort, "Improved air gap permeance model to characterise the transient behaviour of electrical machines using magnetic equivalent circuit method," *International Journal of Numerical Modelling: Electronic Networks, Devices and Fields*, vol. 33, no. 5, p. e2749, 2020.

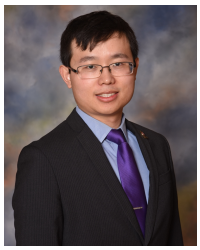

Baoyun Ge (S'13-M'18) received the B.S. in electrical engineering from Southeast University, Nanjing, China in 2012 and the Ph.D. Degree in electrical engineering at the University of Wisconsin-Madison, USA, with the Wisconsin Electric Machines and Power Electronics Consortium (WEMPEC) in 2018. Dr. Ge is now with C-Motive Technologies Inc., a start-up company developing capacitively coupled power conversion technologies. Dr. Ge's interests include electric machines, power electronics and high performance electromagnetic computation. Dr. Ge received the first place paper award and third place thesis award from IEEE Industry Application Society (IAS) in 2017 and 2019 respectively.

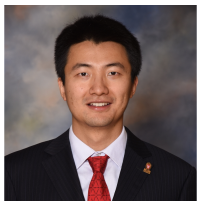

Wenbo Liu (S'14-M'19) received the B.S. in Electrical and Electronics Engineering from Xian Jiaotong University in 2012, and the Ph.D. degree in Electrical Engineering from University of Wisconsin-Madison, with the Wisconsin Electric Machines and Power Electronics Consortium (WEMPEC) in 2019. He is now a research engineer with Ford Research and Advance Engineering. Dr. Liu's research interests including electrical machine design and control for high power density applications.

Jianning Dong (S'10-M'17) received the B.S. and Ph.D. degrees in electrical engineering from Southeast University, Nanjing, China, in 2010 and 2015, respectively. Then he worked as a post-doc research fellow at McMaster Automotive Resource Centre (MARC), McMaster University, Hamilton, Ontario, Canada. He is now an Assistant Professor at the Delft University of Technology. His main research interests are design, modelling and control of electromechanical systems.

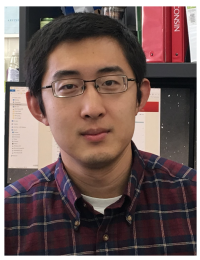

Mingda Liu (S'16-M'20) received BS degree and engineering degree in electrical engineering in 2015 from National Institute of Applied Sciences of Lyon (INSA-Lyon), France, MS and PhD degree in 2017 and 2020, both in electrical engineering, from the University of Wisconsin-Madison, Madison, WI, USA. He worked as research assistant at the Wisconsin Electric Machines and Power Electronics Consortium (WEMPEC), Madison, WI, USA. He is now working at Carpenter Technology Corp. as application engineer. His research focus is on the electromagnetic and thermal design of electric machines.

TABLE III: Winding and Bar Current Extracted from Line-Start for Torque Evaluation in Figure 7.

T_L	Stator Winding, [A]			Rotor Bar, [A]													θ_r
[N-m]	i_a	i_b	i_c	i_{r1}	i_{r2}	i_{r3}	i_{r4}	i_{r5}	i_{r6}	i_{r7}	i_{r8}	i_{r9}	i_{r10}	i_{r11}	i_{r12}	i_{r13}	[m. deg]
1.5	-2.12	-0.65	2.77	-65.9	-47.2	-68.7	-39.3	-15.6	5.82	45.2	68.2	61.7	84.0	13.7	-1.77	-40.2	133.4
3.0	-2.23	-1.54	3.77	104	115	119	105	27.9	-6.04	-94.9	-143	-112	-125	-32.4	-8.63	51.0	219.5
4.5	-2.36	-2.34	4.70	-106	-25.1	35.9	134	183	174	185	31.0	-8.06	-112	-164	-158	-169	353.5
6.0	-2.58	-3.06	5.64	-178	-244	-222	-224	-40.9	9.50	134	206	210	213	148	29.6	-41.2	123.8
7.5	-2.88	-3.95	6.83	-283	-280	-40.5	31.8	204	276	268	265	154	17.5	-83.2	-235	-295	332.5
9.0	-3.33	-3.88	7.21	262	88.7	-12.7	-137	-251	-291	-278	-242	-28.7	58.6	255	310	266	252.1
10.5	-3.68	-4.98	8.66	-216	-330	-360	-342	-257	-27.1	80.4	323	390	360	339	78.2	-39.8	114.9
12.0	-4.00	-5.14	9.15	37.0	-82.7	-340	-398	-370	-349	-103	34.5	200	334	375	366	295	93.1
13.5	-4.46	-5.70	10.2	-25.5	-185	-374	-425	-410	-371	-40.0	88.7	358	419	408	387	169	98.1
15.0	-4.84	-5.36	10.2	43.3	-87.4	-315	-378	-381	-378	-213	-3.57	139	354	408	405	407	89.5